

Intranasal Delivery of circATF7IP siRNA via Lipid Nanoparticles Alleviates LPS-induced Depressive-Like Behaviors

Minzi Ju, Zhongkun Zhang, Feng Gao, Gang Chen, Sibao Zhao, Dan Wang, Huijuan Wang, Yanpeng Jia, Ling Shen, Yonggui Yuan,* and Honghong Yao*

Major depressive disorder (MDD) is a prevalent mental disorder that significantly impacts social and psychological function, but no effective medication is currently available. Circular RNAs (circRNAs) have been reported to participate in the pathogenesis of MDD which are envisioned as promising therapeutic targets. However, nonviral-based delivery strategies targeting circRNA against MDD are not thoroughly investigated. Here, it is identified that circATF7IP is significantly upregulated in plasma samples and positively correlated with 24-Hamilton Depression Scale (HAMD-24) scores of MDD patients. Synergistic amine lipid nanoparticles (SALNPs) are designed to deliver siRNA targeting circATF7IP (si-circATF7IP) into the hippocampus brain region by intranasal administration. Intranasal delivery of SALNP-si-circATF7IP successfully alleviated the depressive-like behaviors in the LPS-induced mouse depression model via decreasing CD11b⁺CD45^{dim} microglia population and pro-inflammatory cytokine productions (TNF- α and IL-6). These results indicate that the level of circATF7IP positively correlates with MDD pathogenesis, and SALNP delivery of si-circATF7IP via intranasal administration is an effective strategy to ameliorate LPS-induced depressive-like behaviors.

rates and serious damage to physical and mental health. Accumulating evidence suggests that over 50 million cases of MDD have been found since the COVID-19 pandemic.^[1] However, there is a lack of effective antidepressant drugs which results in roughly one-third of patients relapsing after current therapeutic strategies.^[2,3]

CircRNA is a type of non-coding RNA with a closed-loop structure and exhibits high abundance in the transcriptomes of eukaryotic genes. The closed-loop structure of circRNA effectively avoids exonuclease degradation and allows circRNA to constantly exist in human bodies, thus making circRNA a promising biomarker and therapeutic target in multiple diseases.^[4] Many circRNAs in the pathogenesis of MDD attracted considerable attention because transcriptome analyses showed aberrant expression of circRNA in the peripheral blood of human and animal models with depression (circSTAG1,^[5] circDCUN1D4,^[6] circRNA5-8S5,^[6] circDYM,^[7] circTFRC,^[8] circTNIK,^[8] etc.). Our previous studies

indicated that circRNAs are engaged in the pathogenesis of MDD. For example, circDYM mechanistically bound to TATA-box binding protein associated factor 1 or miRNA-9

1. Introduction

Major depressive disorder (MDD) is a chronic psychiatric disease characterized by emotional dysfunction, with high recurrence

M. Ju, Z. Zhang, F. Gao, S. Zhao, D. Wang, H. Wang, Y. Jia, L. Shen, H. Yao
Department of Pharmacology
Jiangsu Provincial Key Laboratory of Critical Care Medicine
School of Medicine
Southeast University
Nanjing, Jiangsu 210009, China
E-mail: yaohh@seu.edu.cn

G. Chen, Y. Yuan
Department of Psychosomatics and Psychiatry
ZhongDa Hospital
School of Medicine
Southeast University
Nanjing, Jiangsu 210009, China
E-mail: 101011406@seu.edu.cn

G. Chen, Y. Yuan
Institute of Psychosomatics
School of Medicine
Southeast University
Nanjing, Jiangsu 210009, China

G. Chen
Department of Psychiatry
the Third People's Hospital of Huai'an
Huai'an, Jiangsu 223001, China

H. Yao
Co-innovation Center of Neuroregeneration
Nantong University
Nantong, Jiangsu 226019, China

H. Yao
Institute of Life Sciences
Key Laboratory of Developmental Genes and Human Disease
Southeast University
Nanjing, Jiangsu 210009, China

The ORCID identification number(s) for the author(s) of this article can be found under <https://doi.org/10.1002/adhm.202402219>

DOI: 10.1002/adhm.202402219

which further inhibited microglia activation, suggesting that circRNA participates in MDD pathogenesis by suppressing neuroinflammation.^[7] Using lentivirus- (LV) or extracellular vesicle (EV)-based technologies, our previous studies suggested that circDYM was downregulated among MDD patients, and delivery of circDYM by LV and EV effectively ameliorated depressive-like behaviors in lipopolysaccharides (LPS)-induced and chronic unpredictable stress (CUS)-induced depression mouse models.^[7,9] However, whether interfering with upregulated circRNA also reduced neuroinflammation of MDD remains to be elucidated. Pro-inflammatory response has been implicated in the pathophysiology of MDD.^[10,11] It is well known that MDD is associated with pro-inflammatory immune responses characterized by increased levels of IL-1 β , TNF- α , and IL-6 in microglia populations.^[12–14] The level of pro-inflammatory cytokines corresponds to the activation of microglia with elevated iNOS levels.^[15] Clinical investigations suggested that MDD patients with elevated pro-inflammatory cytokine are less likely to respond to conventional antidepressant drugs.^[16] Hence, interfering with central immune responses by targeting circRNA can potentially address the unmet clinical needs of patients with MDD.

Although viral vectors can deliver gene editing technology to the central nervous systems (CNS), researches claimed that gene delivery based on lentivirus and EVs possessed certain limitations, such as biological toxicities,^[17] heterogeneity,^[18] and physicochemical instabilities that impeded the clinical translation of circRNA-targeted therapies. Lipid nanoparticles (LNPs) are well-established gene delivery systems that maximize nucleic acid drug loading through electrostatic interactions between nucleic acids and ionizable/cationic lipids.^[19] LNPs are often considered safe and stable drug delivery systems that are suitable for clinical translation. Recent advances in LNP structures suggest that the development of organ-specific targeting of LNPs can be achieved by adding selective organ targeting (SORT) molecules among LNP components.^[20] However, it is unknown whether such engineered LNPs will be delivered to the CNS for MDD treatment. In this study, a series of synergistic amine lipid nanoparticles (SALNPs) using a combination of cationic and ionizable amine lipids were developed to improve the delivery efficiency of siRNA to the brain.^[21]

On the other hand, the delivery efficiency of brain-targeted drugs was significantly limited by the blood-brain barrier (BBB).^[22] To bypass BBB and avoid the first-pass effect, intranasal administration was applied as a non-invasive route for neurological therapeutics.^[22] Previous studies indicated that intranasal administration of antidepressant drugs allows quick therapeutic responses compared with intravenous injection of the same drug candidate.^[23] In clinical investigations, esketamine nasal sprays successfully reduced depressive symptoms (active suicidal ideation and treatment-resistant depression) among patients with MDD (NCT03097133, NCT04338321).^[24,25] Therefore, intranasal administration was envisioned as a reliable and promising drug delivery strategy for MDD treatment. Here, engineered SALNPs intranasally delivered siRNA to inhibit the level of circATF7IP in mouse brains, which is newly identified and upregulated during MDD pathogenesis. With the addition of cationic lipid, we demonstrated that these SALNPs containing single ionizable lipid enhanced brain delivery efficiency of si-circATF7IP compared with traditional LNPs. Furthermore, downregulation

of circATF7IP alleviated depressive-like behaviors in the LPS-induced depression mouse model by inhibiting microglia activation as well as pro-inflammatory cytokine productions, providing an innovative approach to treat MDD using novel LNP-based gene delivery and circRNA therapy.

2. Results and Discussion

2.1. CircATF7IP Level was Upregulated in Patients with MDD and Positively Correlated to MDD Pathogenesis

Based on circRNA microarray studies, 4 circRNA (circATF7IP, circZBTB25, circPARN, and circKIAA0319L) were newly found to be upregulated in plasma samples from patients with MDD compared with health controls (HCs) (Figure 1A; Table S1–S5, Supporting Information). The average copy number of circATF7IP was the highest among those upregulated circRNAs (437 copies μL^{-1} of circATF7IP, 237 copies μL^{-1} of circZBTB25, 187 copies μL^{-1} of circPARN and 142 copies μL^{-1} of circKIAA0319L in plasma). In addition, level of circATF7IP exhibited the highest correlation to HAMD-24 scores ($r = 0.431$, $p = 0.0001$) compared with other three circRNAs (circZBTB25: $r = 0.424$, $p < 0.001$, circPARN: $r = 0.360$, $p < 0.001$, circKIAA0219L: $r = -0.161$, $p = 0.085$) (Figure 1B–D; Figure S1 and Tables S6 and S7, Supporting Information). These findings encouraged us to focus on the circATF7IP in our current study although we couldn't rule out the function of other three circRNAs, which will be elucidated in our future study. Patients with mood disorders including bipolar depression (BD), bipolar mania (BM), and schizophrenia (SCZ) were recruited. The demographic information of patients is presented in Table S8 (Supporting Information). It is also noticeable that the level of circATF7IP was significantly upregulated in MDD patients but not in patients with other psychiatric disorders, suggesting the specificity of circATF7IP upregulation in MDD patients (Figure 1E). In addition, the receiver operating characteristic (ROC) curve was applied to evaluate the diagnostic performance of circRNA, circATF7IP was able to differentiate MDD patients from HCs with high sensitivity (75.9%) and specificity (85.5%) in MDD diagnosis (Figure 1F). To assess the predictive value of circATF7IP level for MDD outcome, we evaluated the level of circATF7IP in plasma samples collected within two weeks after hospitalization. Patients who achieved a reduction rate of 50% or more in HAMD-24 scores after antidepressant treatment were categorized as the group with good outcomes.^[26] In Figure 1G,H, the level of circATF7IP exhibited a significant reduction compared to MDD patients before treatment in the good outcome group (Table S9, Supporting Information). ROC curve was plotted based on the change in the value of the circATF7IP between admission and 2 weeks post-treatment to predict the outcome, resulting in an area under the curve (AUC) value of 0.741 (Figure 1I). Given that circRNAs have been detected in plasma high-throughput sequencing data, we proceeded to investigate its potential downstream regulatory mechanisms. Six miRNAs were narrowed to circATF7IP via the CircInteractome database, and the potential miRNAs targeting genes were predicted by the microRNA Data Integration Portal (mirDIP).^[27] Subsequently, these target genes were intersected with depression-related genes in the DisGeNET database, resulting in a total of 92 common target genes. Finally, inputting these 92

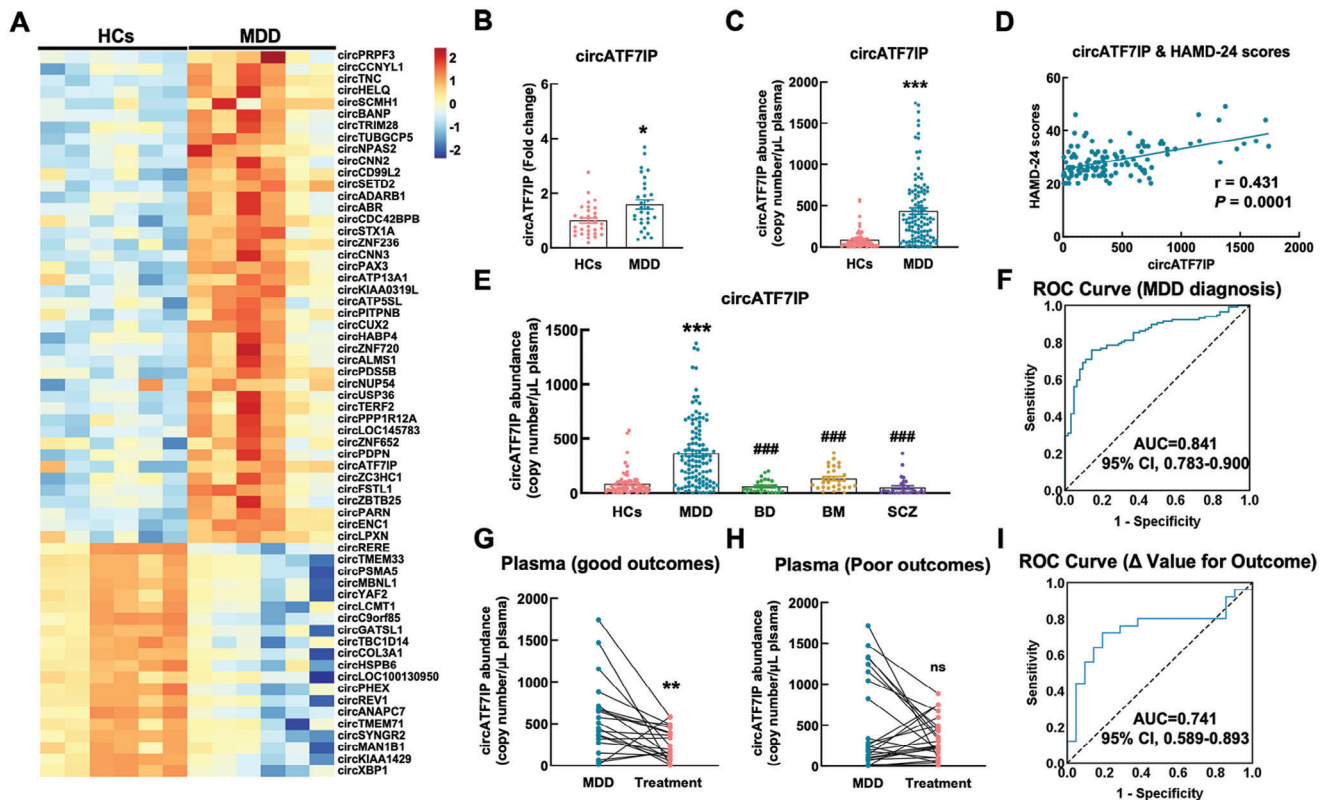


Figure 1. Discovery and validation of circATF7IP in plasma samples from MDD. A) CircRNA microarray revealed the level of circRNAs in HCs and patients with MDD. Red represents high relative expression, blue represents low relative expression. B) Relative expression of circATF7IP in plasma (30 HCs versus 30 MDD). C) Copy numbers per microliter of circATF7IP in HCs and patients with MDD (62 HCs versus 116 MDD). D) Correlation analysis of the level of circATF7IP and HAMD-24 scale in patients with MDD. E) Copy numbers per microliter of circATF7IP in plasma samples from HCs ($n = 62$) and patients with MDD ($n = 116$), BD ($n = 27$), BM ($n = 30$), and SCZ ($n = 29$). F) ROC analysis of circATF7IP in terms of MDD diagnosis. G, H) CircATF7IP abundance in plasma samples from MDD patients who exhibited good outcomes (reduction from baseline of $> 50\%$) and poor outcomes (reduction from baseline of $< 50\%$) two weeks of treatment ($n = 45$). I) ROC analysis was calculated and based on the Δ value outcome (copy number/ μL after two weeks of treatment minus copy number/ μL at admission) of circATF7IP. * $p < 0.05$, ** $p < 0.01$, *** $p < 0.001$ versus HCs group. ### $p < 0.001$ versus MDD group. All data was presented as mean \pm SEM. HCs: health controls. MDD: major depressive disorder. BD: bipolar depression. BM: bipolar mania. SCZ: schizophrenia. ROC: Receiver operating characteristic.

target genes into the DAVID database allowed us to obtain pathway enrichment results for KEGG and GO analysis.^[28,29] KEGG and GO analysis predicted that circATF7IP participated in the inflammatory response pathway and pathogenesis of depression (Figure S2, Supporting Information).^[30] Finally, circATF7IP was elevated in both hippocampal tissue and plasma of the chronic unpredictable stress (CUS)-induced mouse model, which was consistent with the results predicted by microarray results based on samples of MDD patients (Figure S3, Supporting Information).

Our study indicated that circATF7IP was significantly upregulated in the plasma samples from patients with MDD, enabling the MDD-related change of circATF7IP for the application in clinical research into the diagnosis and outcome of MDD. Intriguingly, further correlation analysis indicated that the level of circATF7IP consistently correlated with the clinical symptoms of MDD. Based on absolute qPCR and ROC analysis, we found that circATF7IP was only upregulated in patients with MDD but not with other psychiatric disorders. We found circATF7IP with superior diagnostic and outcome correlation power with AUC over 0.7. Although the role of circATF7IP in human bod-

ies has not been discovered yet, our bioinformatic analysis revealed that circATF7IP highly participated in depression-related biological events in the brain (Figure S2, Supporting Information), and circATF7IP upregulation in the brain was also verified in CUS-induced depressed mice (Figure S3, Supporting Information). Taken together, the average copy number of circATF7IP was mostly increased with the highest correlation to HAMD-24 scores among those upregulated circRNAs. Thus, in this study, we first focused on this circATF7IP and hypothesized that downregulation of circATF7IP in the brain could alleviate depressive-like behaviors as the treatment of MDD.

2.2. Formulation and Characterization of LNPs and SALNPs

To enhance the efficiency of circATF7IP delivery, LNPs and SALNPs with different ionizable lipids DLin-MC3-DMA (MC3, NT1-O14B, SM-102) were designed and formulated to deliver siRNA downregulating circATF7IP (Figure 2A,B,C; Table S11, Supporting Information). To test their capability of siRNA encapsulation and delivery efficiency, MC3 and SM-102 lipids were

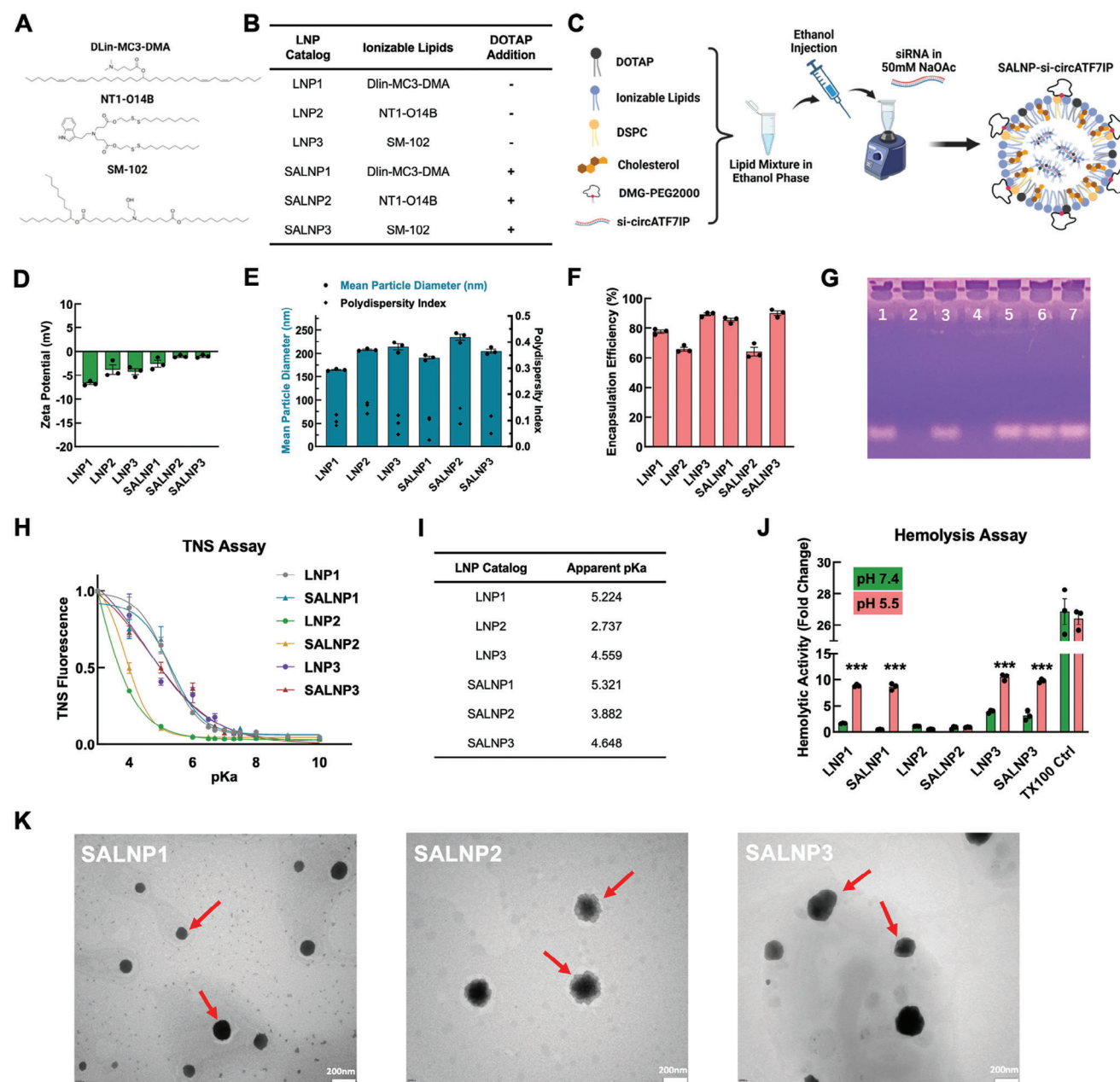


Figure 2. Preparation and characterization of SALNPs encapsulating si-circATF7IP. A,B) DLin-MC3-DMA, NT1-O14B, and SM-102 were individually used to fabricate LNPs and SALNPs. C) LNPs and SALNPs were formulated by ethanol injection of lipid mixture into siRNA phase. D) Zeta potential of LNPs and SALNPs. E) Mean particle diameters of LNPs and SALNPs. F) si-circATF7IP encapsulation efficiency (EE %) in LNPs and SALNPs as determined by Ribogreen RNA quantification kit and reagent. G) si-circATF7IP encapsulation by SALNPs as determined by 1% agarose gel electrophoresis (1: Free siRNA, 2: SALNP1-siRNA, 3: SALNP2-siRNA, 4: SALNP3-siRNA, 5: SALNP1-siRNA + TX100, 6: SALNP2-siRNA + TX100, 7: SALNP3-siRNA + TX100). H,I) TNS assay determined the apparent pKa of LNPs and SALNPs. J) Hemolysis assay identified the pH-dependent ability for membrane disruption by these ionizable LNPs and SALNPs. *** $p < 0.001$ in different pH value. K) TEM images of SALNP1, SALNP2, SALNP3, scale bar: 200 nm. All data was presented as mean \pm SEM, $n = 3$. LNP: Lipid nanoparticle. SALNP: Synergistic amine lipid nanoparticle.

included as standard ionizable lipids for RNA delivery, and NT1-O14B lipid was also included due to its brain-targeted property according to previous literature.^[31,32] Our previous work suggested that LNP containing 1.5% molar percentage (mol %) of DOTAP substantially enhanced oligonucleotide delivery without significant cytotoxicity.^[33] Therefore, the additional 1.5% mol %

of DOTAP was incorporated into the traditional LNP structure as SALNP formulation. Here, with a nitrogen-to-phosphate (N:P) ratio of 6, all types of LNPs and SALNPs possessed slightly neutral surface charges after siRNA encapsulation (Figure 2D). However, MC3-based LNP (LNP1) exhibited a smaller particle size of 160 nm compared with NT1-O14B-based (LNP2) or

SM-102-based (LNP3) LNPs (Figure 2E). Further investigation on the siRNA encapsulation efficiency (EE %) indicated that LNP1 and LNP3 maintained over 80% siRNA EE % whereas LNP2 only partially encapsulated siRNA (60%–70% EE %). Similar results were also observed among three SALNPs where NT1-O14B-based SALNP failed to encapsulate most of si-circATF7IP (Figure 2F,G). Furthermore, the addition of DOTAP in SALNPs elevated the apparent pKa compared with traditional LNPs containing MC3, NT1-O14B, or SM-102. However, we found that the apparent pKa for NT1-O14B-based LNP was below 4 even in the SALNP structure (Figure 2H,I). It is possible that such low pKa contributed by NT1-O14B weakened the membrane fusion property of LNP2 and SALNP2 when they were trapped inside endosomes (Figure 2J). TEM images revealed smooth surfaces on SALNP1 and SALNP3. However, SALNP2 exhibited tooth surface which may be attributed to steric configuration of partial siRNA binding by NT1-O14B (Figure 2K). Synthesized LNPs and SALNPs maintained consistent particle sizes for up to 60 days (Figure S4, Supporting Information). In addition, the EE % of si-circATF7IP in SALNP3 did not significantly reduce, suggesting that si-circATF7IP was stably encapsulated into SALNP3 without release when storing at 4 °C for 60 days (Table S12 Supporting Information). However, the EE % of si-circATF7IP gradually decreased in SALNP1 and SALNP2, suggesting that these two SALNPs did not stably encapsulate si-circATF7IP during long-term storage. This can be attributed to their low pKa profile and trace amine-based branched lipid structure which eventually resulted in low electrostatic interactions with siRNA and irregular LNP surface structure. Therefore, SALNP3 was preferred to encapsulate si-circATF7IP for further studies.

2.3. SALNP3-si-circATF7IP Successfully Downregulated the Level of circATF7IP In Vitro

Based on circRNA sequencing results, we identified that sequences of human and murine circATF7IP were highly overlapped, suggesting that a single siRNA oligonucleotide potentially downregulated both human and murine circATF7IP which can be a favor for clinical translation from animal models to human trials. Here, we designed si-circATF7IP based on the 33-nt overlapped sequences on human and murine circATF7IP (Figure 3A). Cytotoxicities of LNPs and SALNPs were first tested in the RPMI-2650 human nasal epithelial cell line. No significant cytotoxicity was observed when cells were treated with LNP-si-circATF7IP or SALNP-si-circATF7IP at 50 nM or 200 nM concentration (Figure 3B), and delivery of si-circATF7IP successfully downregulated human and murine circATF7IP in A172 and HT22 cells (Figure 3C,D). Using Cy5-labelled si-circATF7IP, we found that SALNPs enhanced delivery of si-circATF7IP in BV-2 cells compared with traditional LNPs, and SALNP3 exhibited the highest si-circATF7IP delivery efficiency (Figure 3E). It is noticeable that the low siRNA EE % by NT1-O14B lipid did not hinder siRNA delivery efficacy in LNP2 and SALNP2 compared with other LNPs and SALNPs, suggesting that NT1-O14B lipid still utilized its branched lipid structure to facilitate endosomal escape and siRNA release intracellularly.^[34] In this work, ionizable lipids with more branched aliphatic chains like NT1-O14B or SM-102 showed better siRNA delivery efficiency

compared with MC3-based LNPs based on cellular uptake studies. Such results were consistent with other reports comparing the RNA delivery efficiency between MC3-based lipids and other ionizable lipids.^[35,36]

Further transfection of si-circATF7IP using SALNP3 showed significant downregulation of circATF7IP in normal and LPS-stimulated BV-2 cells (Figure 3F). The protein level of TNF- α and IL-6 decreased in LPS-stimulated BV-2 cells after treatment with SALNP3-si-circATF7IP. Meanwhile, downregulation of *Tnf- α* and *Il-6* mRNA was only observed in LPS-stimulated BV-2 cells but not normal BV-2 cells (Figure 3G,H; Figure S5, Supporting Information).^[37,38] These suggested that circATF7IP downregulation inhibited pro-inflammatory cytokine levels. Previous studies indicated that transcription factor STAT3 was able to regulate the level of cytokines TNF- α and IL-6.^[39] In normal and LPS-stimulated BV-2 cells, the total level of STAT3 did not significantly change after treatment with SALNP3-si-circATF7IP. However, increased cytoplasmic STAT3 level and decreased nuclear STAT3 level were observed in LPS-stimulated BV-2 cells after treatment with SALNP3-si-circATF7IP, suggesting that circATF7IP downregulation in BV-2 cells by SALNP3-si-circATF7IP inhibited STAT3 translocation to nucleus to facilitate the levels of TNF- α and IL-6 (Figure 3I–K). Additional studies were performed in primary microglia to evaluate the effect of SALNP3-si-circATF7IP on the inflammatory response. The level of Iba-1 was significantly decreased in LPS-stimulated primary microglia after treatment with SALNP3-si-circATF7IP (Figure 3L). The levels of iNOS, TNF- α , and IL-6 were decreased only in LPS-stimulated primary microglia after treatment with SALNP3-si-circATF7IP (Figure 3M–O). These again suggested that SALNP3-si-circATF7IP inhibited the activation of LPS-stimulated microglia.

2.4. SALNPs Enhanced Brain Delivery of si-circATF7IP Compared with Traditional LNPs

To validate and screen the optimal LNPs or SALNPs for brain delivery of si-circATF7IP, DiR-labelled LNP1, LNP2, and LNP3 were administered into mice via intranasal administration. Based on IVIS imaging for mouse whole bodies, all types of LNPs successfully delivered si-circATF7IP (Figure 4A; Figure S6A, Supporting Information). Although without statistical significance, intranasal administration of LNP3 containing SM-102 exhibited higher si-circATF7IP delivery efficiency compared with that of LNP1 and LNP2 which utilized MC3 and NT1-O14B ionizable lipids (Figure 4B). The major organ where LNPs or SALNPs accumulated was still the liver as shown in Figure S6B,C (Supporting Information) and other published reports,^[40,41] however, we noticed that the addition of DOTAP in SALNPs formulations enhanced si-circATF7IP delivery to mouse brains compared with traditional LNPs without DOTAP (Figure 4C–E). This phenomenon was consistently observed between LNPs and SALNPs using three different ionizable lipids, with SALNP3 formulations showing the highest DiR fluorescent signals in the mouse brains compared with other SALNPs formulations (Figure 4F; Figure S6D, Supporting Information). As shown in Figure S7 (Supporting Information), the fluorescent signals of DiR were recorded and quantified at different time points

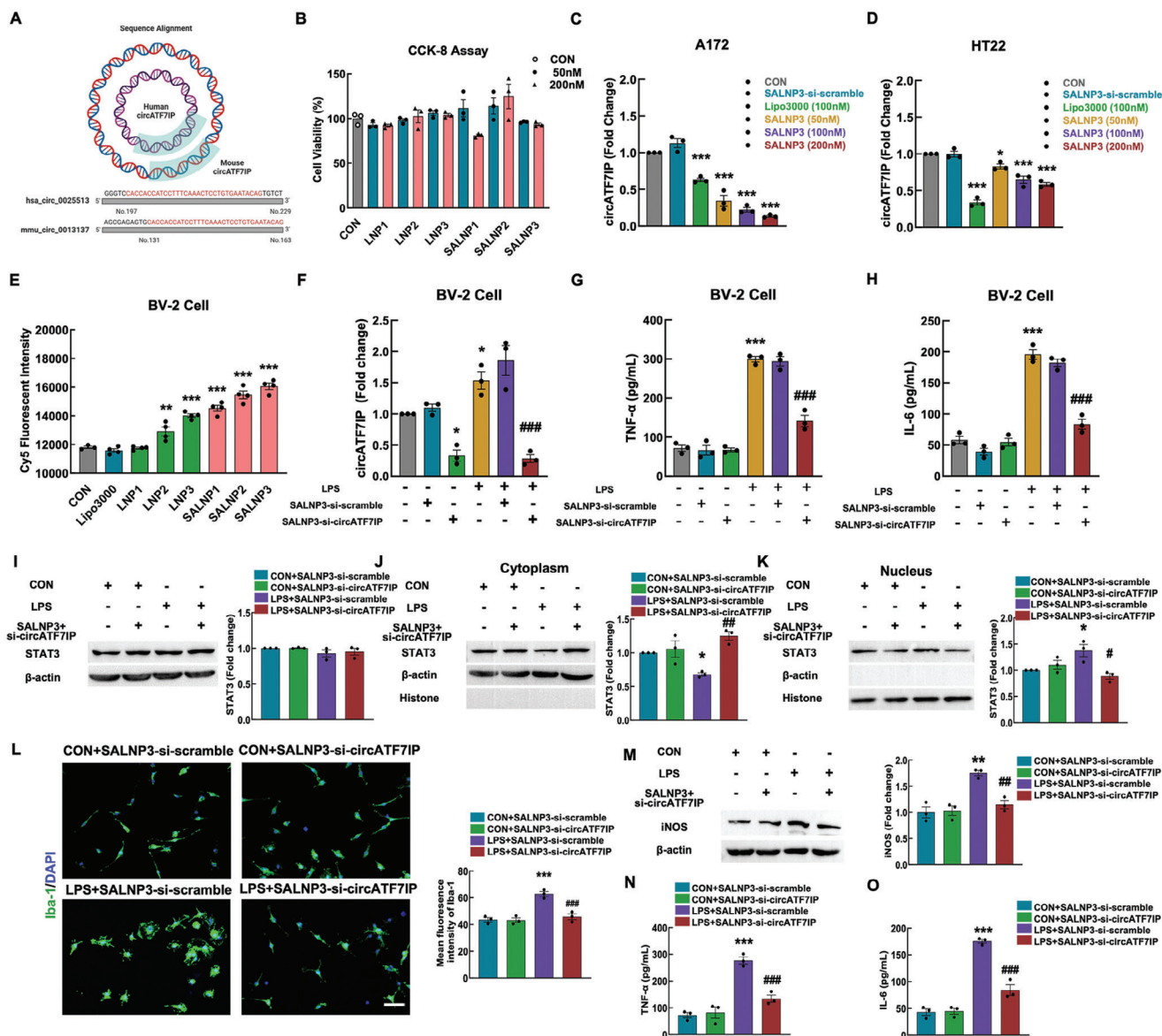


Figure 3. Cell uptake and circATF7IP downregulation by SALNP3-si-circATF7IP. A) Design of siRNA targeting both human and murine circATF7IP. B) CCK-8 assay determined the cytotoxicity of LNPs-si-circATF7IP and SALNPs-si-circATF7IP. C, D) The level of circATF7IP in A172 and HT22 cells was determined by RT-qPCR after treatment with SALNP3-si-circATF7IP or SALNPs-si-circATF7IP. E) Cell uptake ability of LNPs-si-circATF7IP or SALNPs-si-circATF7IP was determined by fluorescence of Cy5-si-circATF7IP. F) The level of circATF7IP was determined by RT-qPCR, the level of TNF- α (G) and IL-6 (H) was determined by ELISA assay after treatment with SALNP3-si-circATF7IP and LPS-stimulated BV-2 cells for 48 h. I–K) Representative western blots of STAT3 protein levels (I) and cytoplasmic (J) or nuclear (K) localization of STAT3 in BV-2 cells with or without treated with LPS (100 ng mL⁻¹) and SALNP3-si-circATF7IP. L) The immunofluorescence staining of Iba-1 and quantitative analysis of mean fluorescence intensity of Iba-1 in primary microglia cells, scale bar: 100 μ m. M) Representative western blots of iNOS protein levels in primary microglia cells. The level of TNF- α (N) and IL-6 (O) was determined by ELISA assay after treatment with SALNP3-si-circATF7IP in LPS-stimulated primary microglia cells for 48 h. All data was presented as mean \pm SEM, $n = 3$. * $p < 0.05$, ** $p < 0.01$, *** $p < 0.001$ versus CON group in A172, HT22, BV-2 or primary microglia cells. # $p < 0.05$, ## $p < 0.01$, ### $p < 0.001$ versus untreated groups in LPS-stimulated BV-2 or LPS-stimulated primary microglia cells.

(0, 0.5, 1, 2, 4, 8, 12, 24, 48, 72 h) after intranasally administered with 0.5 mg kg⁻¹ of si-circATF7IP encapsulated by SALNP3. DiR fluorescence reached the maximum at 4 h post-treatment and gradually decreased to its minimum after 24 h. Such kinetic profiles of SALNP3 were consistent with those from other literature using lipid-based nanoparticles to intranasally deliver RNA therapeutics.^[40,41] Free DiR was intranasally administered

at the same concentration as that of DiR for SALNP fluorescent labeling, but the free DiR group did not exhibit quantifiable fluorescent signals compared with the DiR-labeled SALNP3 group. Considering the highest brain delivery efficiency of si-circATF7IP by SM-102-based SALNP, SALNP3 was chosen to evaluate the therapeutic efficacy of si-circATF7IP via SALNP delivery.

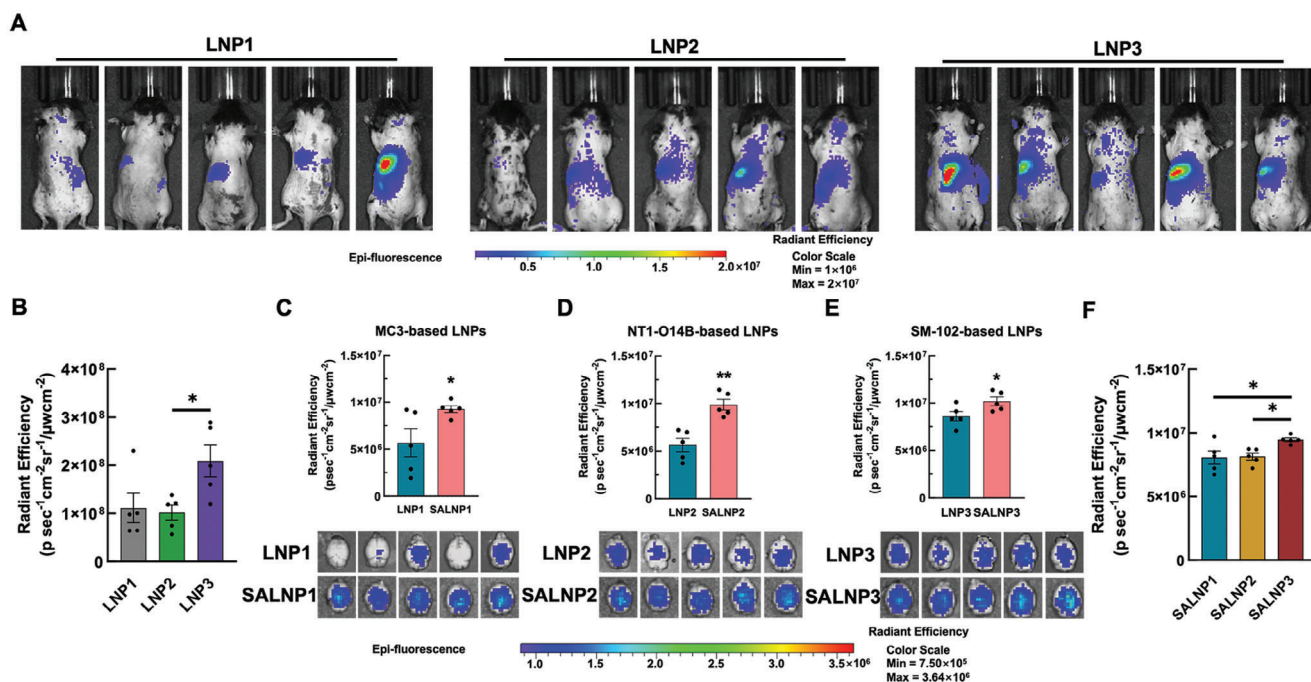


Figure 4. Delivery efficiency of si-circATF7IP by LNPs versus SALNPs in mouse brain. A,B) IVIS images and DiR fluorescence quantification of anesthetized mice after intranasally administered with DiR-labelled LNP1-si-circATF7IP (MC3 Lipid), LNP2-si-circATF7IP (NT1-O14B lipid), and LNP3-si-circATF7IP (SM-102 lipid). C–E) Organ distribution images of DiR-labelled LNPs and SALNPs in mouse brain. F) Fluorescence quantification of DiR-labelled SALNPs in mouse brains. All data was presented as mean \pm SEM, $n = 5$. * $p < 0.05$ and ** $p < 0.01$.

Recent evidence indicated that SORT LNPs containing a combination of functional lipids altered the specific organ-target properties in the liver, lung, and spleen.^[42] Our previous finding also suggested that LNPs with extra cationic lipid components enhanced oligonucleotide delivery in vitro.^[33] In this study, SALNPs, defined as the addition of 1.5% mol % DOTAP in LNPs, overall increased siRNA EE % by shifting pKa to neutral compared with standard LNPs with three different ionizable lipids. As a result, intranasal administration of SALNPs significantly improved siRNA delivery efficiency to mouse brains without altering selectivity to other major organs. In this case, SALNPs with DOTAP lipid might have altered their biological properties after intranasal administration. These could be attributed to decreased protein corona formation and rapid clearance by peripheral phagocytic cells such as macrophages.^[43,44] Nevertheless, we showed that SALNPs were a superior platform for intranasal administration and brain delivery of si-circATF7IP compared with traditional LNPs.

2.5. SALNP3-si-circATF7IP Alleviated Depression-Like Behaviors in LPS-Induced Mice

An LPS-induced depression mouse model was established to evaluate the therapeutic efficacy of SALNP3-si-circATF7IP (Figure S8, Supporting Information). After intraperitoneally injecting LPS for five consecutive days, mice exhibiting depressive-like behaviors (including reduced sucrose preference and increased immobility time) were selected as subsequent subjects for SALNP3-si-circATF7IP or fluoxetine treatments

(Figure 5A; Figure S8, Supporting Information). Here, circATF7IP was significantly upregulated in the brains of LPS-induced depressed mice. After treatment, the downregulation of circATF7IP was only contributed by SALNP3-si-circATF7IP but not SALNP3 components. Furthermore, circATF7IP was also downregulated in plasma and liver samples of mice treated with SALNP3-si-circATF7IP (Figure 5B; Figure S9, Supporting Information). Depressive-like behavior tests after the treatment of SALNP3-si-circATF7IP indicated that depressed mice exhibited increased sucrose uptake (Figure 5C), decreased immobility time (Figure 5D,E), and more interest in exploring the central region, but no significant effect on locomotion was observed after treatment in the motion trajectory map and corresponding heat map from the open field test (Figure 5F–I). These results suggested that downregulating circATF7IP by SALNP3-si-circATF7IP alleviated LPS-induced depressive-like behaviors.

2.6. SALNP3-si-circATF7IP Reduced Pro-Inflammatory Immune Responses in LPS-Induced Depression-Like Mice

Reduced pro-inflammatory immune responses were also observed along with circATF7IP downregulation when depressed mice were treated with SALNP3-si-circATF7IP. Specifically, *Thf- α* and *Il-6* mRNA were significantly downregulated in brain hippocampal tissues from mice treated with SALNP3-si-circATF7IP compared with LPS-induced mice (Figure 6 A,B). Consistent with the above finding, decreased TNF- α and IL-6 cytokines (<100 pg mL⁻¹) were also observed in plasma samples from mice treated with SALNP3-si-circATF7IP (Figure 6C,D). As

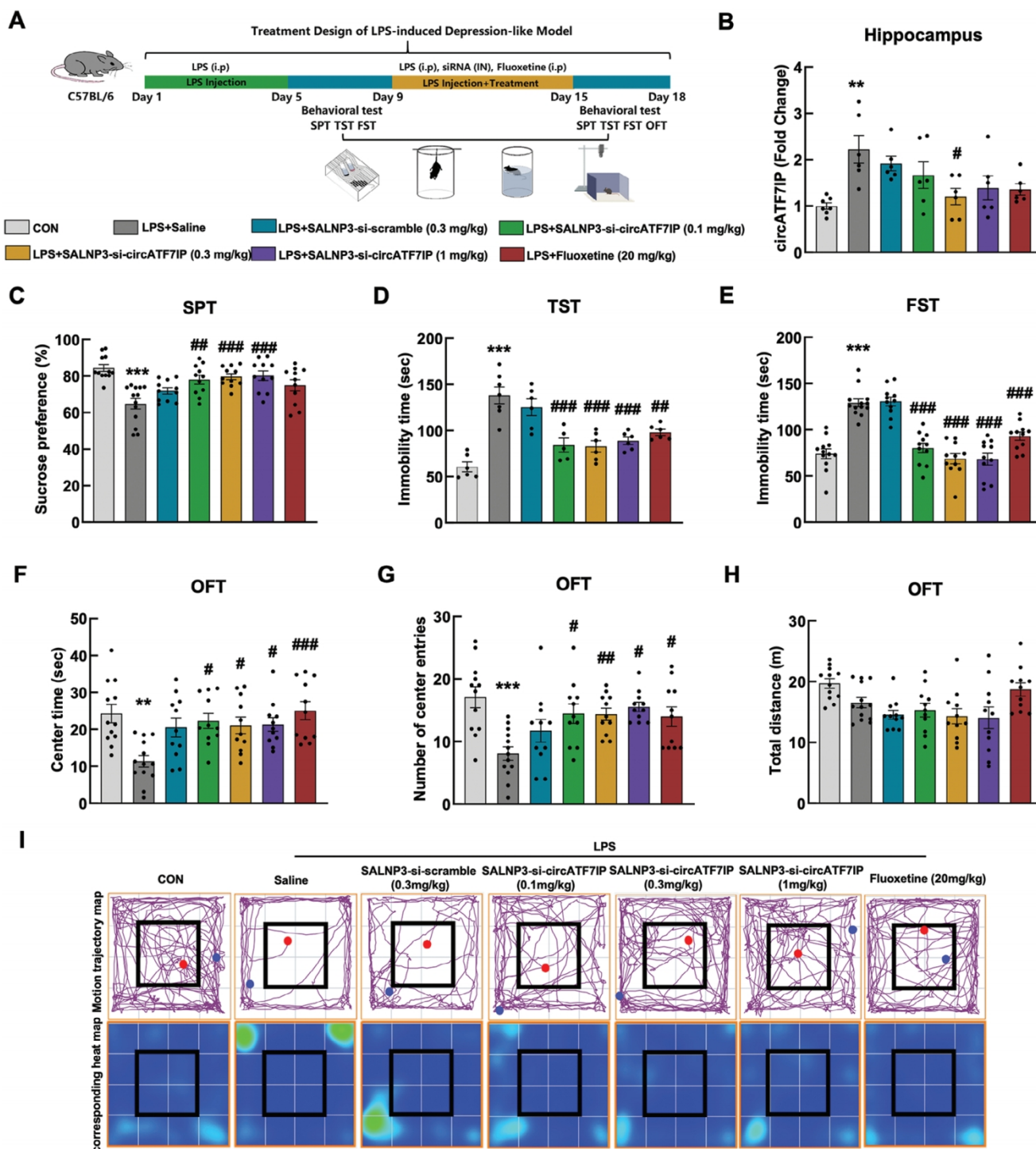


Figure 5. Therapeutic effects of SALNP3-si-circATF7IP against depressive-like behaviors in LPS-induced depression-like mice. A) Establishing LPS-induced depression-like mice and treatment courses. B) CircATF7IP level in hippocampus from LPS-induced mice treated with SALNP3-si-circATF7IP or fluoxetine. All data was presented as mean \pm SEM, $n = 6$. C–H) SALNP3-si-circATF7IP ameliorated depressive-like behaviors in LPS-induced mice as measured by SPT, TST, FST, and OFT. I) The motion trajectory map and corresponding heat map of each group in the OFT. All data was presented as mean \pm SEM, $n = 11$ –13. ** $p < 0.01$, *** $p < 0.001$ versus CON group. # $p < 0.05$, ## $p < 0.01$, and ### $p < 0.001$ versus LPS+ Saline group. SPT: sucrose preference test. TST: tail suspension test. FST: forced swim test. OFT: open field test.

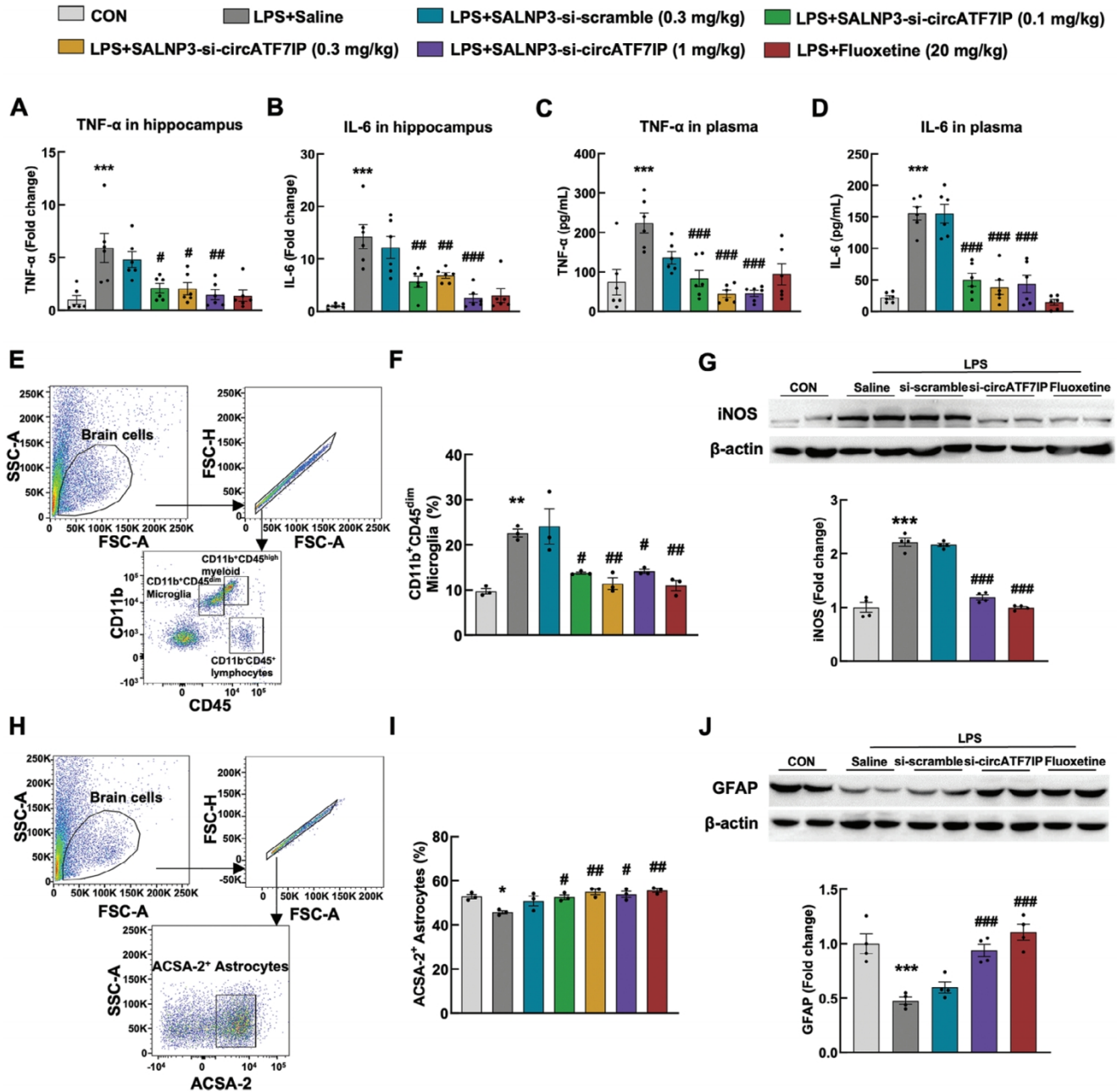


Figure 6. SALNP3-si-circATF7IP reduced pro-inflammatory immune responses in LPS-induced depression-like mice. A,B) RT-qPCR results of *Tnf-α* and *Il-6* mRNA levels in mouse hippocampus. C,D) The level of TNF-α and IL-6 in mouse plasma samples was determined by ELISA. E–G) Changes in CD11b⁺CD45^{dim} microglia populations and iNOS levels in mouse brains after treatment with SALNP3-si-circATF7IP or fluoxetine. H–J) Changes in ACSA-2⁺ astrocyte populations and GFAP levels in mouse brains after treatment with SALNP3-si-circATF7IP or fluoxetine. All data was presented as mean ± SEM, *n* = 4–6. **p* < 0.05, ***p* < 0.01, ****p* < 0.001 versus CON group. #*p* < 0.05, ##*p* < 0.01, ###*p* < 0.001 versus LPS+ Saline group.

microglia are the primary regulators of neuroinflammation, SALNP3-si-circATF7IP treatment decreased the percentage of CD11b⁺CD45^{dim} microglia population and iNOS levels in LPS-induced mice (Figure 6E–G).^[45] Research indicated that a decreased number of astrocytes was observed during the progression of depression.^[46] Here, the number of ACSA-2⁺ astrocytes was decreased in LPS-induced depressed mice, and increased ACSA-2⁺ astrocytes population and GFAP protein level were ob-

served in LPS-induced mice treated with SALNP3-si-circATF7IP. LPS stimulation to mice generally induced inflammatory activation of astrocytes concomitant with increased expression of GFAP when LPS was intraperitoneally administered within 7 days.^[47,48] However, in our study, LPS was intraperitoneally administered once every day for 5 days to induce a depressive model, and LPS was continuously administered during depression-like behavior tests for 4 days. For the depressive mice,

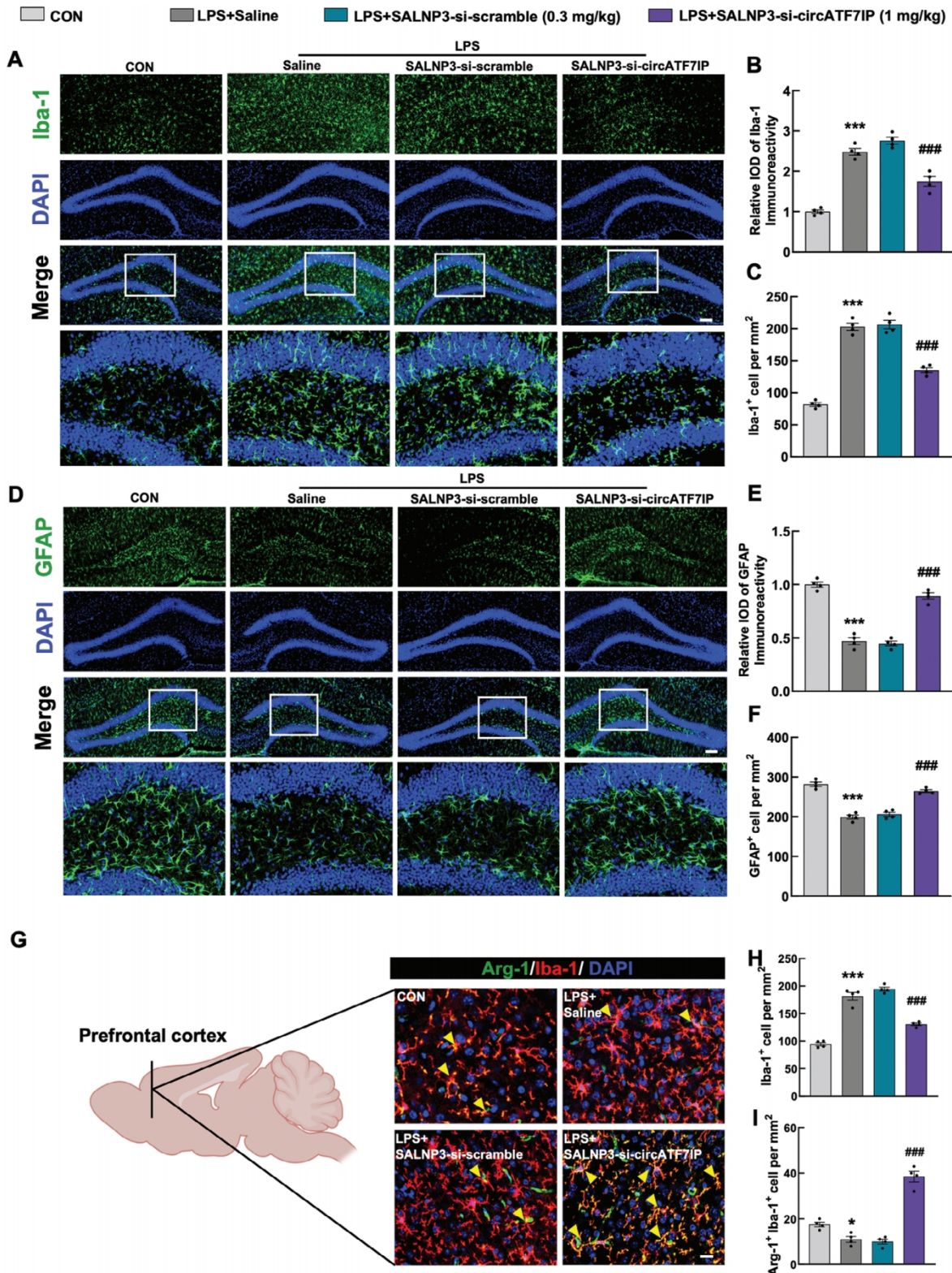


Figure 7. SALNP3-si-circATF7IP attenuated microglial activation and alleviated astrocyte loss dysfunction and attenuated microglial activation to reduce pro-inflammatory immune responses in LPS-induced depression-like mice. A–C) SALNP3-si-circATF7IP attenuated microglial activation in the LPS-induced mouse hippocampus. Representative images of microglial immunostaining for Iba-1 A), scale bar: 100 μ m. Relative IOD of Iba-1 immunoreactivity B), the number of Iba-1⁺ cell C). D–F) SALNP3-si-circATF7IP alleviated astrocyte loss dysfunction in the LPS-induced mouse hippocampus.

they were separated into six groups to evaluate the therapeutic efficacy of SALNP3-si-circATF7IP. LPS was intraperitoneally administered once every day during the 6-day treatment course. Therefore, in our study, intraperitoneal administration of LPS for 15 days induced depressive-like behaviors with a typical pathological manifestation of astrocyte dysfunction characterized by the decreased number of GFAP-positive cells in LPS-treated mice compared with the control group (Figure 6H–J). Our findings are consistent with a previous study that the level of GFAP was decreased in mice for LPS administration over 21 days.^[49] Taken together, these results indicated that downregulating circATF7IP alleviated depression-like behaviors by reducing pro-inflammatory immune responses among glial cells. Lastly, the treatment of SALNP3-si-circATF7IP did not exhibit significant organ toxicities based on H&E histology, suggesting that the SALNP3 strategy was generally regarded as a safe approach for intranasal administration of siRNA payloads (Figure S11, Supporting Information).

Intranasal drug administration holds significant potential in CNS therapeutics with several clinical advantages including non-invasive and simple procedures, enhanced drug bioavailability, and reduced systemic side effects.^[50] Intranasal administration is widely considered a non-invasive approach for drug delivery to the brain by bypassing BBB.^[23,50] However, whether these strategies can be used for siRNA-based MDD therapeutics remains unclear. In previous studies, intranasal administration of antagomirs and siRNA alleviated depressive-like behaviors in depressive-like mouse models.^[51,52] However, these studies lack efficient drug delivery systems to facilitate intracellular delivery of therapeutic agents. Here, intranasal delivery of si-circATF7IP by SALNPs successfully ameliorated LPS-induced depression-like behaviors in depressed mice. Although downregulation of circATF7IP was also observed in mouse livers and plasma samples after treatment, no significant cytotoxicity and organ toxicities were observed based on H&E-stained histology. These results suggested a non-invasive and practical therapeutic strategy against MDD.^[9,53,54] CircATF7IP downregulation by SALNP3-si-circATF7IP also contributed to alleviating neuroinflammation by inhibiting microglial activation as well as pro-inflammatory cytokine (TNF- α and IL-6) production which were consistent with our findings in bioinformatic analysis and cell-based assays. Neuroinflammation directly induces depressive-like behaviors where microglia are overactivated and astrocytes are degenerated.^[45,55,56] In this study, the astrocyte population was also decreased in LPS-induced depressed mice but restored after treatment with SALNP3-si-circATF7IP or fluoxetine. Decreased neuroinflammation in depressed mice by SALNP3-si-circATF7IP was also characterized by a decreased number of CD11b⁺CD45^{high} myeloid cells and CD11b⁻CD45⁺ lymphocytes in mouse brains (Figure S10, Supporting Information).

Previous studies indicated that circRNAs regulated activities of microglia and astrocytes which further contributed to depressive-like behaviors. For example, circDYM mechanistically bound to

TATA-box binding protein associated factor 1 or miRNA-9 which further inhibited microglia activation to alleviate depression-like behaviors. CircSTAG1 increased m⁶A methylation of fatty acid amide hydrolase (FAAH) messenger RNA and promoted FAAH degradation, which further attenuated astrocyte dysfunction and depressive-like behaviors induced by CUS.^[7,9,5] Although further exploration is required to elucidate the biological mechanism of circATF7IP in MDD, our results suggested that downregulating circATF7IP by SALNP3-si-circATF7IP alleviated LPS-induced depression-like behaviors by balancing brain microenvironment involving multiple brain cell types.

2.7. SALNP3-si-circATF7IP Alleviated Neuroinflammation in the Hippocampus and Prefrontal Cortex (PFC) in LPS-Induced Depression-Like Mice

To investigate the neuroinflammation in depression after treatment with SALNP3-si-circATF7IP, immunofluorescence staining was performed to evaluate the levels of Iba-1 and GFAP in the hippocampus in depressed mice. SALNP3-si-circATF7IP treatment significantly attenuated microglial activation, as indicated by the decreased activated microglia (Iba-1 positive) cells in the hippocampus of mice (Figure 7A–C). In addition, we observed that GFAP-positive cells were decreased in the hippocampus of LPS-induced mice while significantly increased after treatment with SALNP3-si-circATF7IP (Figure 7D–F).

Arginase-1 (Arg-1) serves as an anti-inflammatory and neuroprotective biomarker in the microglia, and previous literature reported that the level of Arg-1 was decreased in the depressive-like mouse model.^[57,58] Other reports indicated that the PFC region was consistently impaired in MDD.^[59] To evaluate the change in Arg-1 level in the PFC region after treatment, the immunofluorescence colocalization of Arg-1 and Iba-1 were determined in the prefrontal cortex microglia in brain slices from LPS-induced depressed mice after being treated with SALNP3-si-circATF7IP. The colocalized immunofluorescent signals of Arg-1 and Iba-1 significantly increased in mice with the treatment of SALNP3-si-circATF7IP (Figure 7G–I). These results indicated that treatment with SALNP3-si-circATF7IP increased the level of anti-inflammatory marker Arg-1, suggesting that the increased level of Arg-1 in concord with decreased levels of pro-inflammatory cytokines in mice brains eventually alleviated the depressive-like behaviors in the LPS-induced mouse depression model.

3. Conclusion

Depression severely impairs patients' social and psychological performance. The lack of RNA-based therapies impedes the clinical therapeutic outcomes of depression, especially MDD. In this study, we identified that circATF7IP was upregulated in patients with MDD and positively correlated with depression-like behaviors in MDD patients. Here we proposed a novel

Representative images of astrocyte immunostaining for GFAP (D), scale bar: 100 μ m. Relative IOD of GFAP immunoreactivity (E), the number of GFAP⁺ cell (F). G–I) Representative images of immunofluorescence colocalization of Arg-1 and Iba-1 in the prefrontal cortex (G), scale bar: 20 μ m. The number of Iba-1⁺ cell (H) and the number of Arg-1⁺ Iba-1⁺ cell (I). All data was presented as mean \pm SEM, $n = 4$. * $p < 0.05$ and *** $p < 0.001$ versus CON group. ### $p < 0.001$ versus LPS+ Saline group.

gene delivery strategy based on intranasal administration of si-circATF7IP by SALNPs. Although the detailed molecular mechanism of circATF7IP in MDD remains to be further illustrated, we suggested that SALNP3-si-circATF7IP successfully downregulated circATF7IP and ameliorated depression-like behaviors in the LPS-induced mouse depression model. The current study further sheds light on the therapeutic potential of SALNPs in circRNA-targeted therapies against MDD.

Ethical Statement

Ethical approval for humans was granted by the Clinical Research Ethics Committee of ZhongDa Hospital, Southeast University (ID: 2020ZDSYLL247-P01 and 2022ZDSYLL348-P01) for this study. Two prospective multi-cohort clinical studies (ChiCTR2200061705 and ChiCTR2300069304) were registered on the Chinese Clinical Trial Registry (<http://www.chictr.org.cn>). Animal procedure was approved by the Institutional Animal Care and Use Committee of the Medical School, Southeast University, Nanjing, Jiangsu, China (approval ID 20211027004).

Supporting Information

Supporting Information is available from the Wiley Online Library or from the author.

Acknowledgements

The authors warmly thank Dr. Jinbing Xie for kindly providing access to BeNano 180 Zeta Pro (Dandong Bettersize Instruments Ltd., China) for data acquisition. Figures in the manuscript and table of content were created with BioRender.com. This work was supported by The Science and Technology Innovation 2030-Major Project of the Ministry of Science and Technology of China (2021ZD0202904/2021ZD0202900), The National Natural Science Foundation of Distinguished Young Scholars (82025033), The National Natural Science Foundation of China (82230115), The Natural Science Foundation of Jiangsu Province (Grant No. BK20241311), The Fundamental Research Funds for the Central Universities (2242024K40041), and The Start-up Research Fund of Southeast University (RF1028623361).

Conflict of Interest

The authors declare no conflict of interest.

Author Contributions

M.J., Z.Z. contributed equally to this work. H.Y. and Z.Z. conceptualized the project; Z.Z., M.J. performed methodology; Z.Z. M.J. and H.Y. acquired software; M.J., F.G., G.C., S.Z. and D.W. performed validation; Z.Z. and M.J. did formal analysis; Z.Z. wrote and prepared the original draft; Z.Z., M.J. and H.Y. wrote, reviewed and edited the final manuscript; H.Y., Y.Y., Y.J., L.S. supervised the project; H.Y. and Z.Z. acquired funds. All authors have read and agreed to the published version of the manuscript.

Data Availability Statement

The data that support the findings of this study are available in the supplementary material of this article.

Keywords

CircRNA, depression, lipid nanoparticle, neuroinflammation, oligonucleotide

Received: June 18, 2024

Revised: August 30, 2024

Published online: September 10, 2024

- [1] D. F. Santomauro, A. M. Mantilla Herrera, J. Shadid, P. Zheng, C. Ashbaugh, D. M. Pigott, C. Abbafati, C. Adolph, J. O. Amlag, A. Y. Aravkin, B. L. Bang-Jensen, G. J. Bertolacci, S. S. Bloom, R. Castellano, E. Castro, S. Chakrabarti, J. Chattopadhyay, R. M. Cogen, J. K. Collins, X. Dai, W. J. Dangel, C. Dapper, A. Deen, M. Erickson, S. B. Ewald, A. D. Flaxman, J. J. Frostad, N. Fullman, J. R. Giles, A. Z. Giref, *Lancet* **2021**, 398, 1700.
- [2] K. S. Kverno, E. Mangano, *J. Psychosoc. Nurs. Ment. Health Serv.* **2021**, 59, 7.
- [3] V. L. Ruberto, M. K. Jha, J. W. Murrugh, *Pharmaceuticals* **2020**, 13, 116.
- [4] X. Liu, Y. Zhang, S. Zhou, L. Dain, L. Mei, G. Zhu, *J. Controlled Release* **2022**, 348, 84.
- [5] R. Huang, Y. Zhang, Y. Bai, B. Han, M. Ju, B. Chen, L. Yang, Y. Wang, H. Zhang, H. Zhang, C. Xie, Z. Zhang, H. Yao, *Biol. Psychiatry* **2020**, 88, 392.
- [6] X. Cui, W. Niu, L. Kong, M. He, K. Jiang, S. Chen, A. Zhong, W. Li, J. Lu, L. Zhang, *Biomark Med.* **2016**, 10, 943.
- [7] Y. Zhang, L. Du, Y. Bai, B. Han, C. He, L. Gong, R. Huang, L. Shen, J. Chao, P. Liu, H. Zhang, H. Zhang, L. Gu, J. Li, G. Hu, C. Xie, Z. Zhang, H. Yao, *Mol. Psychiatry* **2020**, 25, 1175.
- [8] T. An, J. Zhang, Y. Ma, J. Lian, Y.-X. Wu, B.-H. Lv, M.-H. Ma, J.-H. Meng, Y.-T. Zhou, Z.-Y. Zhang, Q. Liu, S.-H. Gao, G.-J. Jiang, *Sci. Rep.* **2019**, 9, 10707.
- [9] X. Yu, Y. Bai, B. Han, M. Ju, T. Tang, L. Shen, M. Li, L. Yang, Z. Zhang, G. Hu, J. Chao, Y. Zhang, H. Yao, *J. Extracell Vesicles* **2022**, 11.
- [10] L. Cui, S. Li, S. Wang, X. Wu, Y. Liu, W. Yu, Y. Wang, Y. Tang, M. Xia, B. Li, *Signal Transduct. Target Ther.* **2024**, 9, 30.
- [11] E. Beurel, M. Touns, C. B. Nemeroff, *Neuron* **2020**, 107, 234.
- [12] J. C. Felger, E. Haroon, T. A. Patel, D. R. Goldsmith, E. C. Wommack, B. J. Woolwine, N.-A. Le, R. Feinberg, M. G. Tansey, A. H. Miller, *Mol. Psychiatry* **2020**, 25, 1301.
- [13] J. J. Liu, Y. Bin Wei, R. Strawbridge, Y. Bao, S. Chang, L. Shi, J. Que, B. S. Gadad, M. H. Trivedi, J. R. Kelsoe, L. Lu, *Mol. Psychiatry* **2020**, 25, 339.
- [14] T. Ali, S. U. Rahman, Q. Hao, W. Li, Z. Liu, F. A. Shah, I. Murtaza, Z. Zhang, X. Yang, G. Liu, S. Li, *J. Pineal Res.* **2020**, 69, e12667.
- [15] Z. Bian, H. Li, Y. Liu, Y. Cao, Y. Kang, Y. Yu, F. Zhang, C. Li, Y. Kang, F. Wang, *Neuropsychiatr. Dis. Treat.* **2021**, 17, 2987.
- [16] W. C. Drevets, G. M. Wittenberg, E. T. Bullmore, H. K. Manji, *Nat. Rev. Drug Discov.* **2022**, 21, 224.
- [17] G. Prakash, A. Shokr, N. Willemsen, S. M. Bashir, S. R. Shin, S. Hassan, *Adv. Drug Deliv. Rev.* **2022**, 184, 114197.
- [18] G. Bordanaba-Florit, F. Royo, S. G. Kruglik, J. M. Falcón-Pérez, *Nat. Protoc.* **2021**, 16, 3163.
- [19] X. Hou, T. Zaks, R. Langer, Y. Dong, *Nat. Rev. Mater.* **2021**, 6, 1078.
- [20] Q. Cheng, T. Wei, L. Farbiak, L. T. Johnson, S. A. Dilliard, D. J. Siegwart, *Nat. Nanotechnol.* **2020**, 15, 313.
- [21] Z. Yang, L. Jian, H. Qiu, C. Zhang, S. Cheng, J. Ji, T. Li, Y. Wang, J. Li, K. Li, *Transl. Psychiatry* **2021**, 11, 526.
- [22] J. Xie, Z. Shen, Y. Anraku, K. Kataoka, X. Chen, *Biomaterials* **2019**, 224, 119491.

- [23] L. Boudieu, M. Mennetrier, P.-M. Llorca, L. Samalin, *Pharmaceutics* **2023**, *15*, 2773.
- [24] A. Reif, I. Bitter, J. Buyze, K. Cebulla, R. Frey, D.-J. Fu, T. Ito, Y. Kambarov, P.-M. Llorca, A. J. Oliveira-Maia, T. Messer, S. Mulhern-Haughey, B. Rive, C. von Holt, A. H. Young, Y. Godinov, *N. Engl. J. Med.* **2023**, *389*, 1298.
- [25] D. F. Ionescu, D.-J. Fu, X. Qiu, R. Lane, P. Lim, S. Kasper, D. Hough, W. C. Drevets, H. Manji, C. M. Canuso, *Int. J. Neuropsychopharmacol* **2021**, *24*, 22.
- [26] Y. Zhang, Y. Kong, X. Liu, H. Gao, Y. Yin, Z. Hou, H. Zhang, H. Zhang, C. Xie, Z. Zhang, Y. Yuan, *J. Magn. Reson. Imaging* **2021**, *53*, 1375.
- [27] T. Tokar, C. Pastrello, A. E. Rossos, M. Abovsky, A.-C. Hauschild, M. Tsay, R. Lu, I. Jurisica, *Nucleic Acids Res.* **2018**, *46*, D360.
- [28] J. Piñero, J. M. Ramírez-Anguita, J. Saüch-Pitarch, F. Ronzano, E. Centeno, F. Sanz, L. I. Furlong, *Nucleic Acids Res.* **2020**, *48*, D845.
- [29] J. Piñero, J. Saüch, F. Sanz, L. I. Furlong, *Comput. Struct. Biotechnol. J* **2021**, *19*, 2960.
- [30] B. T. Sherman, M. Hao, J. Qiu, X. Jiao, M. W. Baseler, H. C. Lane, T. Imamichi, W. Chang, *Nucleic Acids Res.* **2022**, *50*, W216.
- [31] F. Ma, L. Yang, Z. Sun, J. Chen, X. Rui, Z. Glass, Q. Xu, *Sci. Adv.* **2020**, *6*, eabb4429.
- [32] Y. Li, Z. Ye, H. Yang, Q. Xu, *Acta Pharm. Sin. B* **2022**, *12*, 2624.
- [33] Z. Zhang, Y. Huang, J. Li, F. Su, J. C. Kuo, Y. Hu, X. Zhao, R. J. Lee, *Adv. Healthcare Mater.* **2022**, *12*, 2202412.
- [34] X. Han, H. Zhang, K. Butowska, K. L. Swingle, M.-G. Alameh, D. Weissman, M. J. Mitchell, *Nat. Commun.* **2021**, *12*, 7233.
- [35] O. Escalona-Rayó, Y. Zeng, R. A. Knol, T. J. F. Kock, D. Aschmann, B. Slütter, A. Kros, *Biomed. Pharmacother.* **2023**, *165*, 115065.
- [36] F. Ferraresso, A. W. Strilchuk, L. J. Juang, L. G. Poole, J. P. Luyendyk, C. J. Kastrup, *Mol. Pharm.* **2022**, *19*, 2175.
- [37] L. Yao, F. Lu, S. Koc, Z. Zheng, B. Wang, S. Zhang, T. Skutella, G. Lu, *Adv. Sci.* **2023**, *10*, 2303711.
- [38] L. Yao, Y. Ye, H. Mao, F. Lu, X. He, G. Lu, S. Zhang, *J Neuroinflammation* **2018**, *15*, 13.
- [39] Y. Jin, Y. Kang, M. Wang, B. Wu, B. Su, H. Yin, Y. Tang, Q. Li, W. Wei, Q. Mei, G. Hu, V. Lukacs-Kornek, J. Li, K. Wu, X. Yuan, W. Wang, *Signal Transduct. Target Ther.* **2022**, *7*, 52.
- [40] G. Anderluzzi, G. Lou, S. Woods, S. T. Schmidt, S. Gallorini, M. Brazzoli, R. Johnson, C. W. Roberts, D. T. O'Hagan, B. C. Baudner, Y. Perrie, *J. Controlled Release* **2022**, *342*, 388.
- [41] A. Tam, J. Kulkarni, K. An, L. Li, D. Dorscheid, G. Singhera, P. Bernatchez, G. Reid, K. Chan, D. Witzigmann, P. Cullis, D. Sin, C. Lim, *Eur. J. Pharm. Sci.* **2022**, *176*, 106234.
- [42] X. Wang, S. Liu, Y. Sun, X. Yu, S. M. Lee, Q. Cheng, T. Wei, J. Gong, J. Robinson, D. Zhang, X. Lian, P. Basak, D. J. Siegwart, *Nat. Protoc.* **2023**, *18*, 265.
- [43] S. A. Dilliard, D. J. Siegwart, *Nat. Rev. Mater.* **2023**, *8*, 282.
- [44] M. Li, X. Jin, T. Liu, F. Fan, F. Gao, S. Chai, L. Yang, *Nat. Commun.* **2022**, *13*, 4137.
- [45] H. Wang, Y. He, Z. Sun, S. Ren, M. Liu, G. Wang, J. Yang, *J. Neuroinflammation* **2022**, *19*, 132.
- [46] C.-L. Lu, J. Ren, X. Cao, *Biol. Psychiatry* **2024**, <https://doi.org/10.1016/j.biopsych.2024.07.017>.
- [47] W. Li, T. Ali, K. He, Z. Liu, F. A. Shah, Q. Ren, Y. Liu, A. Jiang, S. Li, *Brain Behav. Immun.* **2021**, *92*, 10.
- [48] M. M. Novakovic, K. S. Korshunov, R. A. Grant, M. E. Martin, H. A. Valencia, G. R. S. Budinger, J. Radulovic, M. Prakriya, *Nat. Commun.* **2023**, *14*, 5500.
- [49] S. P. Silva, A. M. Zago, F. B. Carvalho, L. Germann, G. de M. Colombo, F. L. Rahmeier, J. M. Gutierrez, C. R. Reschke, M. D. Bagatini, C. E. Assmann, M. da C. Fernandes, *J. Immunol. Res.* **2021**, *2021*, 7497185.
- [50] Y. Chen, C. Zhang, Y. Huang, Y. Ma, Q. Song, H. Chen, G. Jiang, X. Gao, *Adv. Drug Deliv. Rev.* **2024**, *207*, 115196.
- [51] Z.-F. Deng, H.-L. Zheng, J.-G. Chen, Y. Luo, J.-F. Xu, G. Zhao, J.-J. Lu, H.-H. Li, S.-Q. Gao, D.-Z. Zhang, L.-Q. Zhu, Y.-H. Zhang, F. Wang, *Cerebral Cortex* **2019**, *29*, 1509.
- [52] M. N. Fullana, A. Ferrés-Coy, J. E. Ortega, E. Ruiz-Bronchal, V. Paz, J. J. Meana, F. Artigas, A. Bortolozzi, *Mol. Neurobiol.* **2019**, *56*, 3038.
- [53] X. Qian, Z. Zhong, Y. Zhang, L. Qiu, H. Tan, *Brain Res.* **2024**, *1825*, 148723.
- [54] M. L. Formica, D. A. Real, M. L. Picchio, E. Catlin, R. F. Donnelly, A. J. Paredes, *Appl. Mater. Today* **2022**, *29*, 101631.
- [55] H.-G. Lee, J.-H. Lee, L. E. Flausino, F. J. Quintana, *Sci. Transl. Med.* **2023**, *15*, eadi7828.
- [56] L. A. O'Leary, N. Mechawar, *Glia* **2021**, *69*, 2077.
- [57] A. A. Atta, W. W. Ibrahim, A. F. Mohamed, N. F. Abdelkader, *Inflammopharmacology* **2023**, *31*, 1053.
- [58] J. Zhang, L. Li, Q. Liu, Z. Zhao, D. Su, C. Xiao, T. Jin, L. Chen, C. Xu, Z. You, T. Zhou, *Phytomedicine* **2023**, *113*, 154725.
- [59] D. A. Pizzagalli, A. C. Roberts, *Neuropsychopharmacology* **2022**, *47*, 225.